

The effect of confinement-induced shear on drop deformation and breakup in microfluidic extensional flows

Molly K. Mulligan and Jonathan P. Rothstein

Department of Mechanical and Industrial Engineering, University of Massachusetts, 160 Governors Drive, Amherst, Massachusetts 01003, USA

(Received 19 August 2010; accepted 4 January 2011; published online 11 February 2011)

Droplets of de-ionized water and four aqueous surfactant solutions were generated in oil using a microfluidic flow-focusing device. The morphological developments of the drops in extensional flow and confinement-induced shear flow at various extension rates were studied using a hyperbolic contraction. This novel approach to droplet deformation within a microfluidic device allowed the probing of droplets within a nearly uniform extensional flow. The focus of this work was to study the effect of confinement-induced shear on droplet deformation and breakup in extensional flows. Droplet deformation was found to increase with both increasing capillary number and increasing confinement, for a fixed viscosity ratio of $\lambda=0.1$, with the effect of the shear induced by confinement being quite dramatic. The addition of surfactant to the droplets resulted in the production of tails, which streamed from the rear of the droplets and produced daughter droplets much smaller than the parent droplet. In the partially confined limit, where the flow was purely extensional, a single tail was formed at the center of the droplets trailing edge. With enhanced confinement, shear effects from the wall became important, the droplets were observed to take on a bullet-like shape, and two tails formed at the trailing edge of the droplet. The critical value of the capillary number and confinement needed for the formation of tails varied with the surfactant used. © 2011 American Institute of Physics. [doi:10.1063/1.3548856]

I. INTRODUCTION

Emulsions, which are defined as stable droplets of one immiscible fluid in another, are useful in a range of applications from personal care products such as body wash, to foods such as salad dressing, to the pharmaceutical industry where they can be utilized as drug delivery vehicles, and to the chemical industry where they can be used as microreactors.¹ In addition, the surfaces of dispersed droplets can be utilized for purification of the bulk phase and as templates for assembly of lipids or colloidal particles for novel materials.² Unlike a suspension of solid particles, emulsion droplets are readily deformed under flow because the liquid-liquid interface is mobile.^{3,4} Understanding the deformation and breakup of droplets under flow has been a topic of great interest since Taylor's seminal experiments⁵ and a number of excellent reviews exist in the recent literature.^{6,7}

Bulk emulsions are traditionally formed using high-speed mixing and agitation where stresses generated within the flow are used to break apart an immiscible mixture into small droplets. The size of the drops produced is determined by the strength of the flow as described by the capillary number which can be written a number of ways depending on the flow type

$$\text{Ca} = \frac{U \eta_c}{\sigma_{12}} = \frac{\dot{\gamma} R \eta_c}{\sigma_{12}} = \frac{\dot{\epsilon} R \eta_c}{\sigma_{12}}, \quad (1)$$

where U is the velocity, R is the maximum radius of the drops that do not break, η_c is the viscosity of the continuous phase, $\dot{\gamma}$ is the shear rate, $\dot{\epsilon}$ is the extension rate, and σ_{12} is the interfacial tension between the dispersed and bulk

phases. The critical capillary number for droplet breakup has been shown to be a function of both the character of the flow (shear or extension) as well as the viscosity ratio, $\lambda = \eta_d / \eta_c$. Here η_d is the viscosity of the dispersed phase. The critical capillary number has been found to be significantly smaller in extensional flows than in shear flow with the result that at the same deformation rate, smaller droplets can be produced in extensional flows.⁸ It should be stressed, however, that creating emulsions in this way typically results in a wide distribution of drop sizes. In many applications, control over both the size and the size distribution of such droplets is the critical element in such emulsions.⁹ Recent work has shown that emulsions with nearly monodisperse droplet size distributions can be produced using microfluidic devices.^{10,11}

Several microfluidic techniques have recently been explored for the generation of monodisperse drops including colliding jets, T-junctions, and hydrodynamic flow focusing.¹⁰ The simple shearing cross flow of a continuous phase past a T-junction where a dispersed phase is introduced has been shown to be a simple and effective method of creating stable and monodisperse droplets for a variety of fluid systems.¹²⁻¹⁴ In the coflowing method, droplets are created by focusing a stream of fluid between coflowing immiscible fluids.^{9,15} The formation of a central microthread and tip streaming makes it possible for this method to create small droplets ($<1 \mu\text{m}$) with a limited polydispersity.¹⁶ Additionally, although the flow-focusing geometry is more complex, the nature of the flow has provided more control, allowing very interesting results including the creation of gas microbubbles in a continuous liquid phase,¹⁷ as well as stable multiple emulsions of droplets within the droplets.^{18,19} A re-

cent study reviewed the impact of channel geometry, cross-flowing or coflowing, on stable emulsion creation¹⁸ and showed the advantages of each method. In this study, we have chosen to use hydrodynamic flow focusing to generate droplets with a range of precisely controlled droplet diameters.

Droplet deformation and breakup has been studied in steady flows, such as pure extensional flows, irrotational flows,⁸ shear flows,^{5,20} and combined shear and extensional flows.²¹ The deformation of droplets within emulsions was first studied by Taylor, who noted that the movement of the continuous phase fluid would distort the droplet due to the inertial and viscous forces which acted on the drop surface, while the surface tension would act to keep the droplet spherical.⁵ Studying the deformation and breakup of droplets has led to a more complete understanding of the rheology of emulsions, dynamics of droplet breakup and coalescence, and the motion of droplets in capillaries provides insight into pore scale hydrodynamics for enhanced oil recovery.²²

Surfactants are often used to stabilize emulsions against coalescence because the repulsive interaction between the surfactants on the surface of the droplets prevents it.²³ Surfactants can also aid in droplet creation within a microfluidic device because they reduce the interfacial tension between the dispersed and continuous phases. Additionally, surfactants can lead to the phenomenon of tip streaming as discussed in Refs. 16 and 24.

Droplet deformation and breakup is governed by the capillary number and the interplay between the viscous and surface forces. When the capillary number is large, viscous forces dominate and the initially spherical droplet becomes ellipsoidal and eventually breaks into smaller droplets. Conversely at low capillary numbers, surface forces dominate and the drop remains spherical. In addition to the studies on individual droplets in shear and extensional flows, extensive work has been to study how shear flow affects polydisperse bulk emulsions. For polydisperse emulsions, the capillary number experienced by each droplet will vary. Migler²⁵ used the shear flow between two rotating parallel disks to study the effect of shear and confinement on drop deformation and flow-induced structure in polydisperse emulsions during droplet coalescence. High shear rates were initially used to produce a high concentration of water droplets in oil. At a fixed gap between the disks, a number of distinct transitions were observed as the shear rate was progressively decreased; smaller droplets coalesced into larger droplets, which aligned due to flow into pearl necklace like structures and finally to strings of the dispersed phase fluid. It was also shown that similar transitions were obtained by maintaining a fixed shear rate and decreasing the gap between the plates as the degree of confinement was increased. The string to droplet transition was also seen over a range of viscosity ratios, $0.1 \leq \lambda \leq 10$, and in the case of both a Newtonian and highly elastic continuous phase fluid.²⁵

Vananroye *et al.*²⁶ looked at how a confinement of less than one affects the dynamics of single droplet breakup in shear flows for clean droplets. Using a counter-rotating parallel plate flow cell with a constant gap between the plates of $1000 \mu\text{m}$, drops ranging in diameter from

$160 \leq D \leq 800 \mu\text{m}$ were injected into the matrix fluid individually and sheared over the range of capillary numbers from $0.0 \leq \text{Ca} \leq 0.5$. Confinement is defined as

$$C = \frac{R}{w_2}, \quad (2)$$

where w_2 is the half-width of the gap the droplet is confined in. For droplets with a confinement of $C=0.8$, droplet deformation was enhanced for all viscosity ratios, $0.31 \leq \lambda \leq 2.03$. For droplets with a confinement of $C=0.2$, over the same range of viscosity ratios, droplet deformation was found to match the predictions of the Maffettone and Minale model. In the work of Pathak *et al.*,²⁷ droplets which were strongly confined were found to have deformation enhanced and droplet breakup suppressed by confinement for a viscosity ratio of $\lambda=1$.

The confinement of droplets can also be exploited to enhance or suppress the breakup of droplets. For an unconfined droplet, the critical capillary number for droplet breakup is dependent on the viscosity ratio of the two fluids.⁸ This transition from stable drop to breakup is the result of the imbalance of viscous and interfacial forces.²⁸ For extensional flows, the critical capillary number for breakup for unconfined droplets varies from $0.25 \geq \text{Ca}_{\text{cr}} \geq 0.1$ for viscosity ratios of $10^{-3} \leq \lambda \leq 10^2$ and then becomes constant for $\lambda=3$ at $\text{Ca}_{\text{cr}}=0.1$. For pure shear flows over the same range of viscosity ratios the critical capillary number is $0.35 \leq \text{Ca}_{\text{cr}} \leq 0.58$.⁸ In the work done by Vananroye *et al.*,²⁹ it was found that the critical capillary number for droplet breakup increased with increasing confinement for viscosity ratios of $\lambda < 1$. However, for viscosity ratios of $\lambda > 1$, an increase in droplet confinement led to a decrease in the critical capillary number for droplet breakup.

As described above, much work has been done to study emulsions under shear flow conditions. Droplets within emulsions also often undergo extensional flows in their various industrial uses. For example, a nozzle is essentially an abrupt contraction placing extensional stresses on the fluid being passed through it. In this paper, we explore how extensional flow affects droplet deformation under partial and full confinement using microfluidics on the single drop scale. Little work has been done to study droplets under an extensional flow in the presence of sidewall confinement. According to a recent review by Pipe and McKinley,³⁰ work in microfluidics has included planar hyperbolic contractions like the one utilized here. These systems have been used to measure the extensional rheology of polymeric solutions³⁰ and as a preconditioner to stretch DNA molecules.³¹ Additionally there have been a small number of studies where abrupt contractions were used to deform droplets. These contractions are easier to design and build; however, unlike hyperbolic contractions the droplets do not experience a uniform extension rate throughout the contraction and the comparison to previous unconfined four-roll mill experiments cannot be made directly.³⁰⁻³² Thus, there is still a gap in the fundamental understanding of the process of droplet deformation by extensional flows in complex fluids that this paper seeks to fill.

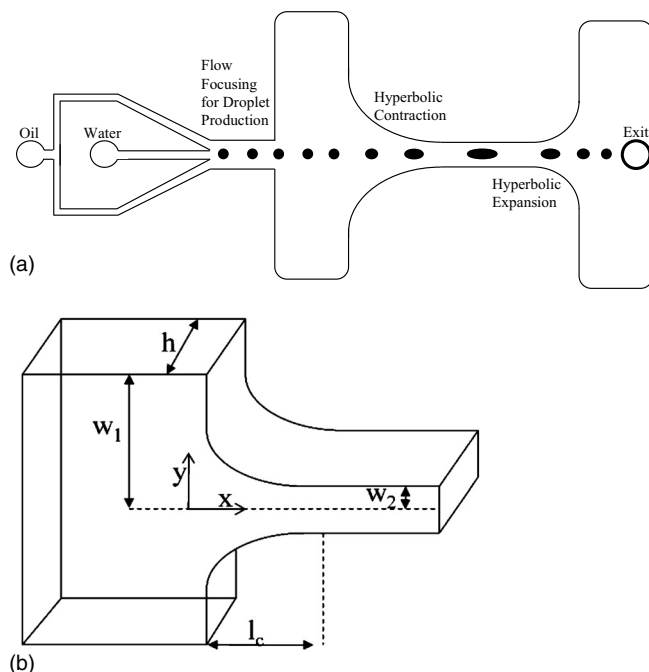


FIG. 1. Schematic diagram of the flow cell used in these experiments. In (a) the entire flow cell is shown, including the hydrodynamic flow-focusing region where droplets are produced and the hyperbolic contraction where they are stretched in a nearly constant extensional flow. In (b) the relevant dimensions of the hyperbolic contraction are shown.

The format of this paper is as follows. First, the experimental methods and design of the hyperbolic contraction are discussed. Next, the results highlighting the effect of confinement on droplets in extensional flows are discussed. Finally, we conclude.

II. EXPERIMENTAL

A. Channel geometry and setup

The experimental flow cell is shown schematically in Fig. 1(a). The flow cell was designed with a flow-focusing geometry to create a steady stream of monodisperse droplets followed by a hyperbolic contraction where droplet deformation and breakup can be measured as a function of extension rate and confinement. The devices were fabricated using standard soft lithography techniques.^{33,34} A computer aided design program, AUTOCAD™, was used to design the microfluidic device. The design was then printed on a high-resolution transparency at 20 000 dpi, thus resulting in features as small as 10 μm . A negative photoresist, SU8 (MicroChem Corporation, Newton, MA), was used to create master wafers for rapid prototyping of the microfluidic devices with channel walls $h=200 \mu\text{m}$ deep.³³ Microfluidic devices are then cast from the master wafer using poly(dimethyl)-siloxane (PDMS, Dow Sylguard 184, Copley, OH). To seal the devices, standard glass microscope slides were spin-coated with a thin layer of PDMS and the molded devices were then bonded to the slides using a simple PDMS-ratio mismatch to provide uniform surface properties within the channels. More details of the specific fabrication procedure can be found in previous work.^{35,36} The flow

TABLE I. The relevant dimensions used for each of type of flow cell used in the experiments.

Type of flow cell	w_1 (μm)	w_2 (μm)	l_c (μm)
FC1	3000	25	2000
FC2	3000	50	1000

through the microchannels is driven by two stepper-motor actuated microsyringe pumps (New Era Pump Systems, NE-500 OEM, Wantagh, NY) using a 500 μl glass syringe (Hamilton, Microliter™ 750, Reno, NV) for the dispersed phase and a 10 ml plastic syringe (BD, plastic Leur-Lok Tip, Franklin Lakes, NJ) for the continuous phase.

In order to investigate the deformation of droplets under an extensional flow and investigate the role of confinement on droplet deformation, a hyperbolic contraction was incorporated into the microfluidic device. A hyperbolic contraction was chosen because the fluid entering the contraction experiences a nearly constant extension rate within the contraction.³² The flow through a hyperbolic contraction has been used to measure the extensional rheology of polymeric fluids for more than 30 years by relating the measured pressure drop across the contraction to the flow rate.^{30,37–39} More recently, the hyperbolic contraction extensional rheometer has been fabricated within microfluidic devices, which due to their small size can be used to probe the rheology of low viscosity fluids in the absence of inertial effects^{30,32} and stretch DNA.³¹ A schematic diagram of the hyperbolic contraction used in these experiments with all the pertinent dimensions labeled is shown in Fig. 1(b). The position of the walls along the hyperbolic contractions is described by the following equation:

$$y = \frac{c_1}{x + \frac{2c_1}{w_1}}, \quad (3)$$

where y is the vertical position within the channel, $c_1=0.025 \text{ mm}^2$ is a design parameter which dictates the strength of the extensional flow, x is the position along the length of the channel, and $w_1=3 \text{ mm}$ is the half-width of the channel before the contraction. The design parameter $c_1=1/2w_2l_c$ can be related to the length of the contraction, l_c , and the final downstream half-width, w_2 . The length of the contraction, l_c , was either 2 or 1 mm depending upon the value of the downstream half-width, which was taken as either $w_2=25 \mu\text{m}$ or $w_2=50 \mu\text{m}$, respectively. The narrower channel is called FC1 and the wider channel is called FC2 and all relevant channel dimensions are summarized in Table I. FC1 and FC2 were used in the study of the water droplets and the cetylpyridinium chloride (CPyCl) solution droplets. FC2 was only used to study the other three surfactant solutions. The upstream half-width w_1 was held constant for all flow cells at $w_1=3 \text{ mm}$. After reaching its minimum width, the contraction is extended for an additional 1.5 mm at a separation of $2w_2$, so that the effect of confinement on droplet breakup can be observed. The contraction is then reex-

TABLE II. The relevant interfacial tensions and viscosities for the various droplet phase fluids used in the experiments.

Fluid	σ (mN/m)	η (mPa s)
Water	19	1
CPyCl	4.8	1
NaOa	5.6	1
CTAB	2.1	1
OTAB	5.6	1

panded through a hyperbolic expansion designed to result in a compression rate which is ten times smaller than that of the contraction.

The fluids are pumped into the flow cell using syringe pumps which impose a constant volumetric flow rate, Q . The result is an average velocity within the channel that increases linearly with position along the length of the contraction,

$$u(x) = \frac{Q}{yh} = \frac{Q}{c_1 h} \left(x + \frac{2c_1}{w_1} \right). \quad (4)$$

Here h is the height of the channel and yh is the cross-sectional area at any given point in the channel. A more detailed solution of the spatially resolved velocity profiles requires numerical simulations and can be found in Oliveira *et al.*³² The extension rate in the channel based on the average velocity in Eq. (4) thus becomes

$$\dot{\epsilon} = \frac{\partial u}{\partial x} = \frac{Q}{c_1 h}. \quad (5)$$

In our microfluidic device, a range of extension rates between $37s^{-1} < \dot{\epsilon} < 2100s^{-1}$ was accessible. Additionally, the total Hencky strain imposed on the fluid can be determined from $\epsilon = \ln(w_1/w_2)$ which for our geometry is equal to $\epsilon_{FC1} = 4.8$ and $\epsilon_{FC2} = 4.1$. The extension rate calculated from Eq. (5) was thus used to recalculate an extensional capillary number, as shown in Eq. (1).

It should be noted that this ideal homogeneous extensional flow does not occur across the entire channel due to the presence of shear near the walls of the hyperbolic contraction. The shear rate is at a maximum at the walls of the channel and decreases to zero at the centerline. At the narrowest point in the hyperbolic contraction the shear rate at the wall can be as much as twice as the extension rate; however, it decreases significantly at wider points of the contraction. Oliveira *et al.*³² showed both experimentally and computationally that a nearly constant extension rate can still be achieved along the centerline of the hyperbolic contraction. In addition, they demonstrated that for over 80% of the channel width, the velocity is essentially constant and can be approximated by the plug flow approximation. In the absence of droplets, our own micro-particle image velocimetry (μ -PIV) data were consistent with these findings. Thus, shear will become increasingly important as the droplet confinement increases and the droplets approach the wall.



FIG. 2. Schematic of how droplet deformation is measured for various deformed droplet shapes.

B. Experimental methods

All experiments were carried out on an inverted microscope (Nikon TE2000-U, Melville, NY) and video data were recorded using a high-speed video camera (Vision Research, Phantom 4.6, Wayne, NJ). The continuous phase fluid for all experiments was Miglyol oil, which has a viscosity of $\mu_c = 10$ mPa s (Miglyol Oil 840, Sasol, Johannesburg, South Africa). The dispersed phase consisted of either de-ionized water or one of four surfactant solutions. The surfactant solutions consisted of 5 mM CPyCl in water, 5 mM hexadecyltrimethyl ammonium bromide (CTAB) in water, 5 mM octyltrimethyl ammonium bromide (OTAB) in water, and sodium oleate (NaOa) in water. The interfacial tension between Miglyol oil 840 and each of the dispersed phase solutions was characterized using a pendant drop experiment (Data-physics, OCA 20, San Jose, CA) and are listed in Table II. In all cases the viscosity ratio was fixed at $\lambda = 0.1$.

The applied flow rate was varied, so that a range of extension rates and extensional capillary numbers could be accessed for the droplets as they entered the contraction. Droplet deformation was measured using IMAGEJTM and quantified using the deformation parameter⁵

$$D = \frac{a-b}{a+b}, \quad (6)$$

where a is the length of the major axis of the ellipse formed when the drop is deformed and b is the length of the minor axis. Droplet deformation was measured as a function of the extensional capillary number and the amount of relative confinement of the drop. Not all droplets remain elliptical in shape. In Fig. 2, we show how each of the droplet shapes is measured to determine the values of a and b . It is important to note that the length of the tails formed at the rear of some drops was not incorporated into the deformation parameter because we felt that would skew the data.

III. RESULTS AND DISCUSSIONS

A. Deformation of water droplets in oil

Our initial measurements studied the deformation of clean water drops in extensional flows. In Fig. 3(a), the deformation parameter as a function of the extensional capillary number for various amounts of relative droplet confinement is shown. Without confinement, the critical capillary number for droplet breakup for a viscosity ratio $\lambda = 0.1$ is $Ca_{cr} = 0.19$.⁸ It can be seen in Fig. 3(a) that the droplet deformation increases with increasing confinement over the entire range of capillary numbers studied for water droplets. In Fig. 3(a), the capillary number increases from $0.005 \leq Ca \leq 0.03$ as one moves from symbols near the bottom to the top at a given confinement. Even for the droplets with a confinement

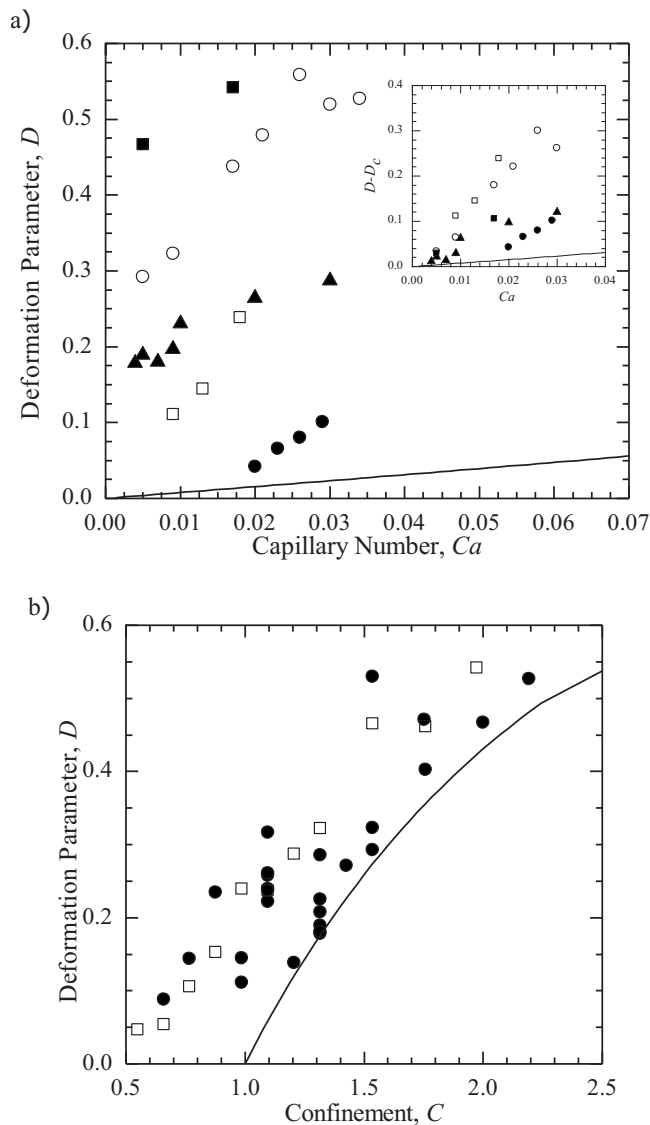


FIG. 3. In (a) the deformation parameter as a function of the extensional capillary number is shown at various confinements for water drops in oil. The strength of the extensional flow is defined by the capillary number and the deformation parameter shows the deviation of a drop from a circle. The data include confinement parameters at $C=0.66$ (●), $C=0.99$ (□), $C=1.3$ (▲), $C=1.5$ (○), and $C=2.0$ (■). The line represents predictions of the Maffettone and Minale model. (b) shows the deformation parameter as a function of the confinement for all capillary numbers studied (●). A capillary number of $Ca=0.02$ is shown by (□). The solid line shows the deformation parameter vs confinement at zero capillary number.

parameter of $C < 1$, significant deformations beyond the unconfined case predicted by droplet deformation models were observed.

In order to try to understand the results from first principles and to help quantify the effects of confinement in these extensional flows, the predictions of the Maffettone and Minale model⁴⁰ for droplet deformation in a homogeneous uniaxial extensional flow in the absence of confinement are superimposed over the data in Fig. 3(a) (clean water droplets) and later in Fig. 8(a) (CPyCl surfactant droplets).

The Maffettone and Minale model⁴⁰ was originally developed in order to determine droplet deformation resulting from an arbitrary flow around a droplet. The model makes

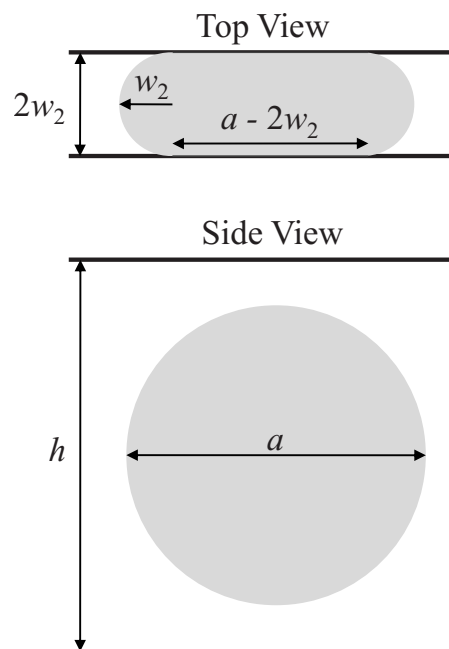


FIG. 4. Schematic diagram illustrating the shape of confined drop at $Ca=0$.

two basic assumptions. First, that the droplet remains ellipsoidal at all time, and second, that the drop does not break up. It is thus only truly applicable in flows below the critical capillary number. MATLAB was used to solve the Maffettone and Minale model under pure extensional flow conditions in order to determine the resulting unconfined drop shape and deformation as a function of extension rate and strain.⁴¹

As expected, even in the presence of confinement, droplet deformation increases monotonically with increasing capillary number. However, as the confinement is increased, greater droplet deformation is observed at a given capillary number. In addition, the onset of deviations of the droplet deformation from predictions of the Maffettone and Minale model occurs at lower capillary numbers with increasing confinement. For the case of $C=0.66$, the data deviate from the predictions of the Maffettone and Minale model at a capillary number of about $Ca=0.016$. For $C=1.0$, the deviation appears to occur just past the onset of flow at about $Ca=0.01$. While for fully confined drops, $C > 1.0$, the data never follow the Maffettone and Minale model. We also see that the slope of the line for deformation versus capillary number at any confinement is greater than that predicted by the Maffettone and Minale extensional model. The larger slope is likely due to the secondary shear effects which are a direct result of confinement and will be discussed in greater detail later. Similar trends of increased deformation with increasing confinement were observed in confined shear flows for viscosity ratios less than $\lambda < 1$.²⁶ Unfortunately, for the microfluidic device used here, it was not possible to approach the extensional capillary number and impose strain necessary to break the water drops in the hyperbolic contraction.⁸ We will, however, show that confinement effects can have a dramatic effect on the critical capillary number for breakup of surfactant coated drops.

For confinement greater than one, the droplets are too large to fit through the contraction without first deforming. The deformation due solely to steric confinement at vanishingly small capillary number can be determined by starting from a simple volume conservation argument. Here we make two assumptions. First, that the flow does not deform the drop, $Ca \ll 1$, and second, that the drop is only confined in the y -direction and not in the z -direction. The deformed drop should thus take on a pancake-like shape shown schematically in Fig. 4. The total volume of the drop compressed between the sidewalls of the throat of the contraction can be estimated as the sum of a cylinder with a diameter $a - 2w_2$ plus a revolved semicircle with diameter $2w_2$ (this is shown schematically in Fig. 4),

$$V = \left[\frac{\pi}{2} (a - 2w_2)^2 w_2 \right] + \left[\pi^2 w_2^2 \left(\frac{a - 2w_2}{2} + \frac{4}{3\pi} w_2 \right) \right]. \quad (7)$$

By volume conservation, the deformed volume must be equal to the undeformed drop volume, $V = 4/3\pi R^3$. Equating these, a rather messy expression for deformation parameter as a function of a confinement factor can be derived in the limit of vanishingly small capillary number, $D_c = f(C)$. Predictions from this model are superimposed over the data in Fig. 3(b) resulting in a lower bound for confined drop deformation. These calculations also suggest that the deformation parameter can be renormalized to remove the deformation due to low capillary number confinement, $D - D_c$, in order to highlight the deformation resulting from the flow only. A plot of renormalized deformation parameter is presented as an inset in Fig. 3(a). The data do not collapse onto a master curve; however, the vertical shift in the data is due to the steric effects at $C > 1$ which are for the most part eliminated. These results demonstrate the important role that confinement plays by not only physically limiting the lateral size of the drop, but by changing the flow type from a pure extensional flow under limited confinement to one of mixed shear and extensional flows in the presence of strong confinement. As we will see, shear flow that sets up between the droplet and the walls of the hyperbolic contraction has a strong effect not only on droplet deformation, but also on droplet breakup.

Vananroye *et al.*^{26,29} noted that in shear flows a confined droplet broke up at a capillary number greater than that predicted for an unconfined droplet with a viscosity ratio less than unity. However, for higher viscosity ratios, $\lambda > 1$, Vananroye *et al.*²⁶ found that confinement promoted droplet breakup. It can also be seen from their work that partially confined droplets ($C = 0.77$) deviated from the predictions of the Maffettone and Minale model, whereas nearly unconfined droplets ($C = 0.2$) undergoing shear forces agreed with the model predictions over the range of capillary numbers studied. To better understand the role of confinement on water drop deformation in extensional flows, the deformation parameter is plotted as a function of confinement in Fig. 3(b). The data show that the droplet deformation increases with increasing confinement for a given capillary number. This observation is made more clear by isolating a single

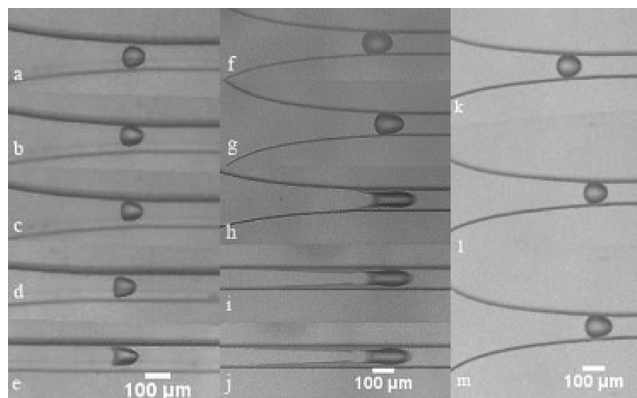


FIG. 5. Droplet deformation for three different types of drops. The capillary number increases from top to bottom in each case. (a)–(e) are 5 mM CPyCl solution droplets with a confinement of $C = 0.77$ and a radius of $r_d = 38 \mu\text{m}$. (a) $Ca = 0.014$. (b) $Ca = 0.024$. (c) $Ca = 0.03$. (d) $Ca = 0.05$. (e) $Ca = 0.08$. (f)–(j) are 5 mM NaOa solution drops and these drops have a confinement of $C = 1.1$ and a radius of $r_d = 55 \mu\text{m}$. (f) $Ca = 0.002$. (g) $Ca = 0.006$. (h) $Ca = 0.016$. (i) $Ca = 0.019$. (j) $Ca = 0.21$. (k)–(m) are water droplets with a confinement of $C = 0.99$ and a radius of $r_d = 49 \mu\text{m}$. (k) $Ca = 0.009$. (l) $Ca = 0.013$. (m) $Ca = 0.018$.

capillary number, $Ca = 0.02$, within the many data sets presented in Fig. 3(b). The general trends in the data agree with those in the literature for confined shear flows.^{8,26} Additionally, the predictions of Eq. (7) for minimum deformation for confinements greater than $C > 1$ are superimposed over the experimental data. All the deformation parameters in Fig. 3(b) were found to be larger than the predicted minimum. For a given capillary number, the difference between the deformation and the zero capillary number limit $D - D_c$ remains positive everywhere, but appears to decrease with increasing confinement. This suggests that the out of plane, z -direction, deformation of the drops increases with increasing confinement and increasing influence of the shear flow.

B. Deformation and breakup of surfactant coated water droplets in oil

Surfactants are often used in emulsions as stabilizers. It is therefore important to understand the role of surfactants on drop deformation and breakup. Surfactants have hydrophobic tails and hydrophilic heads and will self assemble on oil-water interfaces to minimize the free energy of the system, thereby reducing the interfacial tension. On an interface, surfactants are mobile, they can adsorb and desorb very quickly and can be moved around the droplet surface by flow setting up surface tension gradients and inducing Marangoni flows.⁴² This flow-induced gradient in interfacial tension causes clean drops and surfactant covered drops to behave very differently, as can be seen in Fig. 5.

Figure 5 shows two different surfactant solution droplets at the beginning of the hyperbolic contraction at varying capillary numbers and a water drop for comparison. Some droplets in Fig. 5 are shown past the hyperbolic contraction in order to emphasize the tails on the rear of the droplets. Figures 5(a)–5(e) show droplets of CPyCl with an undeformed radius of $r_d = 38 \mu\text{m}$ and a confinement of $C = 0.77$. As the capillary number increases from top to bottom, the drop de-

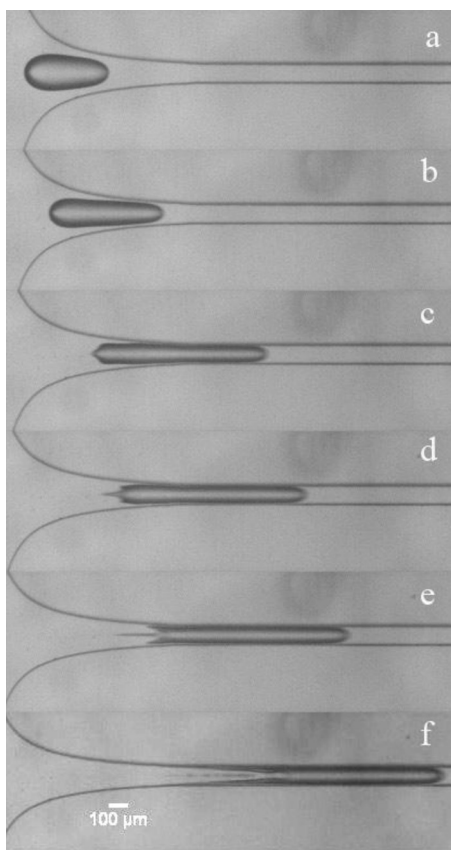


FIG. 6. A time series of images showing tail formation due to extensional stresses placed on the droplets as they enter the hyperbolic contractions. This is a solution of 5 mM NaOa in Migyol oil 840. In (a) the drop is entering the contraction at time $t=0$ ms. In (b) the drop is shown further into the contraction at time $t=1.62$ ms. In (c) the extensional tail is seen beginning to form the back of the drop at $t=3.24$ ms. In (d) the extensional tail is seen at $t=3.82$ ms. In (e) the formation of two other tails due to the confinement of the droplet is shown at $t=4.4$ ms. In (f) the drop is seen as it is out of the contraction and fully confined at $t=5.56$ ms.

formation increases and the droplet shape progresses from an ellipsoid to a bullet and finally to what appears to be a rocket ship shape. The same holds true for the fully confined droplet of NaOa, $C=1.1$, shown in Figs. 5(f)–5(j). In the case of the NaOa the droplet shape transitions from an ellipsoid to a bullet to tail streaming. Tails are not observed for water drops at any capillary numbers or confinements studied. See Figs. 5(k)–5(m) for examples of water droplet deformation. Mietus *et al.*²¹ found similar twin tails when applying an orthogonal shear to macroscopic drops of castor oil in a Couette cell. The process that forms these tails is similar to the process of tip streaming. Tip streaming is a well-understood phenomenon, which occurs due to a surface tension gradient at the tip of a jet or droplet.^{16,43} The surface tension gradient is most likely the result of a surfactant concentration gradient caused by surfactants being swept by the extensional, as in Figs. 6(c) and 6(d), and/or shear flows, as in Figs. 6(e) and 6(f), to the tip/poles of the droplet. Booty *et al.*⁴⁴ performed simulations to show the evolution of tip streaming from the poles of a droplet held in place by a four-roll mill and undergoing zero-Reynolds-number extensional flow. They also showed that in the limit of zero sur-

face diffusion of surfactant, the insoluble surfactants immobilize the surface of a droplet. The movement of the surfactants to the back of the drop causes a large reduction in the surface tension making the formation of sharp, cusp-like interfaces energetically favorable.

As seen in Fig. 5, the shape transitions observed for water droplets and surfactant droplets are quite different. The deformed water droplets are initially spherical before becoming elliptical with increasing capillary number. At larger capillary numbers, water droplets begin to take on a bullet-like shape, with a slightly blunt trailing edge and a rounded leading edge. Surfactant-laden droplets, on the other hand, transition to the bullet-like shape at a much lower capillary number than water droplets do. As the capillary number is further increased, long tails of fluid are pulled first as a single tail from the center of the surfactant-laden drops and then as the drop is more heavily confined two tails form near the wall, as seen in Fig. 6. The location of the two tails near the wall suggests that they are shear induced, while the single tail in the center is extensionally induced. In fact, tails are clearly observed to occur at lower capillary number with increasing confinement. Once these long tails are formed, the surfactant droplets begin to shed material in the form of daughter drops from the tailing edge of the droplet. For the 5 mM CPyCl solution, the bullet shape forms at a capillary number of $Ca=0.005$, whereas the bullet shape for the NaOa is not observed until a capillary number of $Ca=0.006$ and not until $Ca=0.018$ for water. It is important to note that no droplet breakup is observed for water droplets at the confinements and capillary numbers tested in this study. This is not completely unexpected because the capillary number is well below the critical capillary number achieved for unconfined drops.

Inspecting the tails shown in Fig. 6 more closely, we see that the droplet enters the contraction as an ellipsoid with the front of the droplet always being slightly thinner than the rear of the droplet. The droplet continues to extend as it enters the contraction, with a single tail forming on the rear of the droplet indicating the presence of strong extensionally dominated flow at moderate drop confinement. As was seen in four-roll mill extensional flow experiments,⁸ a single tail forms at the rear stagnation point of the droplet, Fig. 6(c). The single tail continues to extend until the tailing edge of the droplet becomes fully confined. At this point in the flow, shear becomes important and two tails form on the end of the droplet next to the walls of the contraction, Fig. 6(e). The single tail is simultaneously observed to detach from the middle of the droplet and break up. As the droplet progresses further into the contraction, the double tails along the walls of the confinement also begin to break up. This transition from the single tail to double tails highlights the complexity of drop deformation in confined extensional flows as the flow transitions from pure extensional to mixed kinematics with increased confinement. It also demonstrates that unlike in shear flows, confinement for viscosity ratios less than 1, $\lambda < 1$, reduces the critical capillary number for drop breakup by as much as an order of magnitude. Note that in unconfined extensional flow critical capillary number for tip streaming is reported as $Ca=0.5$ for $\lambda \leq 0.1$.^{16,45}

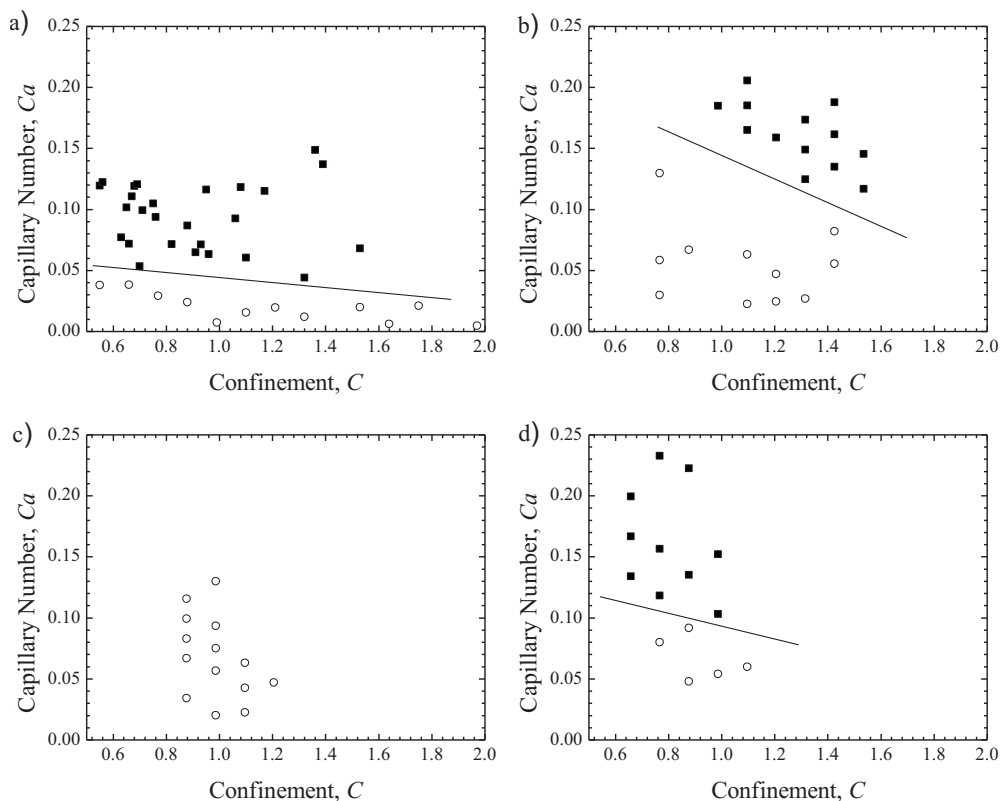


FIG. 7. Phase diagram showing the presence of tails (■) or no tails (○) for the flow of four different surfactant solutions through a hyperbolic contraction. Data are included for (a) 5 mM CPyCl, (b) 5 mM NaOa, (c) 5 mM OTAB, and (d) 5 mM CTAB. A line is superimposed over the data to emphasize the transition from no tails to tails. This line is not quantitative but is only meant to guide the eye.

In Fig. 7, a phase diagram is presented for all surfactant solutions used, which quantifies the transition from droplets which do not have tails to droplets which do have tails from which daughter droplets are streaming. The lines included on the graphs in Fig. 7 are simply meant to guide the eye, they are not meant to be quantitative. It is interesting to note that OTAB solution, like water, does not form tails at the trailing edge of the droplet at any of the capillary numbers or confinements tested. The transition to tail streaming occurs at a different capillary number for each of the surfactant solutions tested. This is likely due to the differences in molecule size and mobility of each surfactant. Smaller molecules diffuse to and along the droplet interface more quickly than the larger molecules.⁴⁶

Since OTAB is the smallest molecule, it is also likely the most mobile. Higher flow rates and capillary numbers are therefore required to produce the same surfactant concentration and surface tension gradients achieved along the droplets populated by the large, less mobile surfactants. Higher capillary numbers could not be reached for the OTAB solution under these experimental conditions. As a result, the OTAB appears to behave more like water drops than the other surfactant solution drops. For the NaOa solution drops, tail formation happens at higher confinement and capillary numbers than for the other surfactant solutions presumably because it is the second smallest and second most mobile molecule.

In Fig. 8 the evolution of droplet deformation through the hyperbolic contraction is shown for a partially and fully

confined droplet. Droplet deformation initially increases as it passes through the contraction. However, in both the partially and full-confined case the deformation asymptotes to a steady state value well before the end of the hyperbolic con-

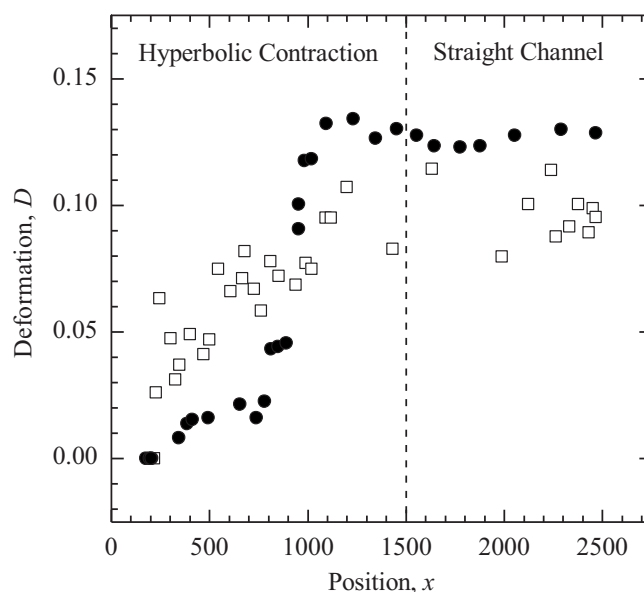


FIG. 8. The deformation parameter D as a function of position x within the channel for CPyCl droplets. The hyperbolic contraction extends from $0 \leq x \leq 1500 \mu\text{m}$. Beyond $x = 1500 \mu\text{m}$ the width of the microfluidic channel is fixed at $w_2 = 50 \mu\text{m}$. The data include a confinement and capillary numbers of $C = 0.66$ and $Ca = 0.034$ (□) and $C = 1.1$ and $Ca = 0.008$ (●).

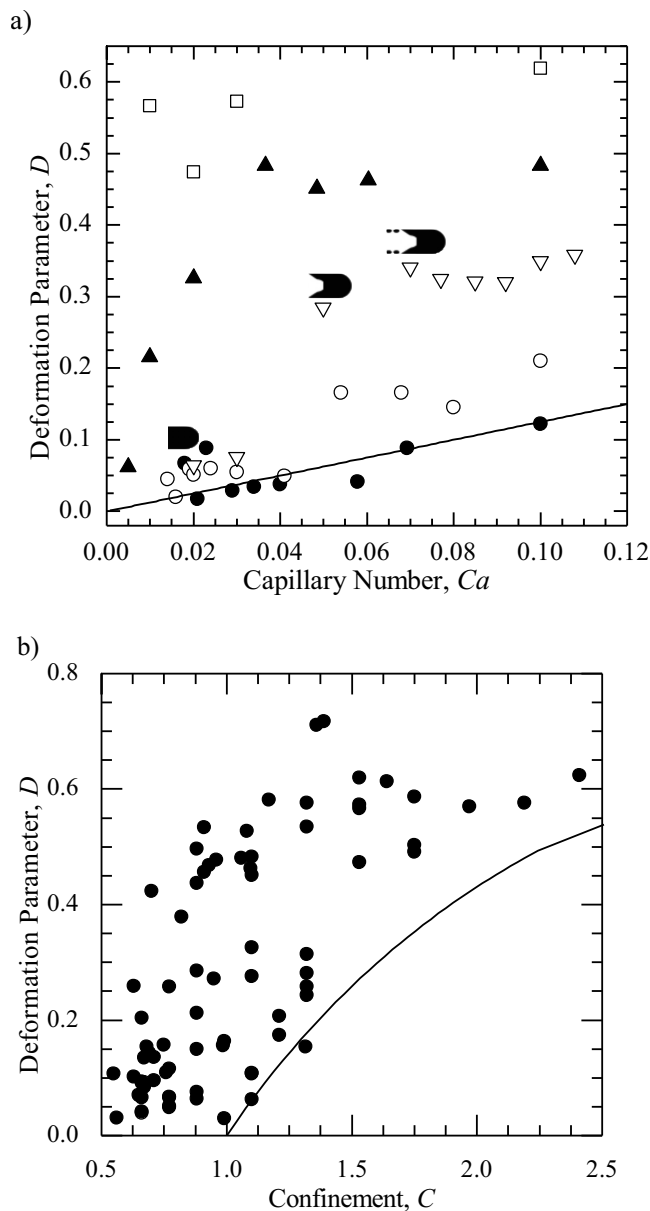


FIG. 9. In (a) the deformation parameter is shown as a function of the capillary number at various confinements for 5 mM CPyCl drops in oil undergoing extensional flows. The strength of the extensional flow is defined by the capillary number and the deformation parameter shows the deviation of a drop from a circle. The data include confinement parameters at $C=0.66$ (●), $C=0.77$ (○), $C=0.88$ (▽), $C=1.1$ (▲), and $C=1.5$ (□). The line shown represents the results of the Maffettone and Minale model for extensional flows. In addition, sketches showing drop shape transitions are superimposed over the $C=0.88$ data. (b) shows the deformation parameter as a function of the confinement for all capillary numbers studied (●).

traction at $x=1500 \mu\text{m}$. For both droplets, the data initially show a first order growth in the droplet deformation leading to an asymptotic steady state value achieved relatively early on in the hyperbolic contraction and well before the start of the downstream straight channel. For the fully confined droplet, $C=1.1$, the initial plateau is close to the predictions of the unconfined Maffettone and Minale model; however, at a position of about $x=750 \mu\text{m}$, a shape transition is observed from an ellipsoidal to a bullet-like shape along with a corresponding jump in the droplet deformation. At the point of the

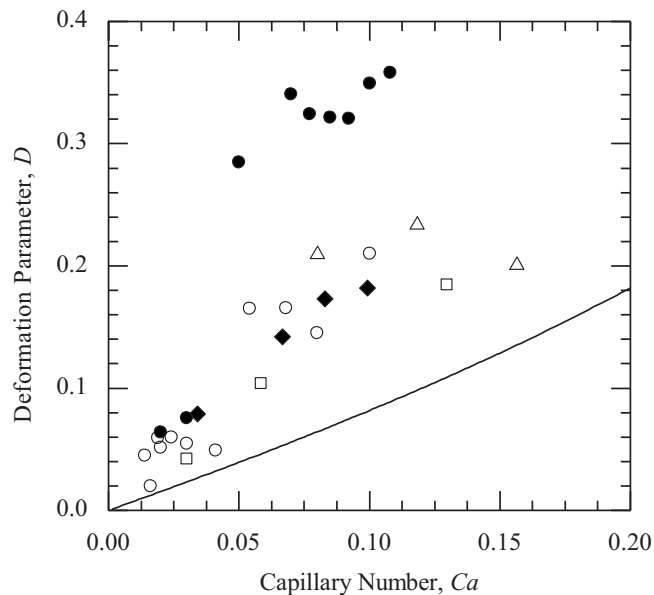


FIG. 10. The deformation parameter is shown as a function of the capillary number at various confinements for the three other surfactant solution drops. The data include the confinement parameter of $C=0.77$ for NaOa (□), CTAB (△), and CPyCl (○) and $C=0.88$ for OTAB (◆) and CPyCl (●). The line shown represents the results of the Maffettone and Minale model for extensional flows.

shape transition, the droplet is at a relative confinement of about $C=0.73$. It is not until a position of about $x=900 \mu\text{m}$ that the droplet becomes fully confined, $C>1$, by the contraction walls. So it is clear that the effects of shear are felt even for partially confined flow.

Figure 9(a) shows the deformation parameter as a function of the capillary number for CPyCl surfactant solution droplets. The trends for the deformation parameter as a function of the confinement are qualitatively similar to those observed for water, with higher deformation parameters at the same capillary number. This disparity is likely due to the flow-induced surface tension gradients present along the surfactant-laden drops. For low partial confinement, the deformation parameter as a function of capillary number seems to follow the Maffettone and Minale model even more closely than the clean water droplets did. However, the droplet deformation is observed to deviate dramatically from the Maffettone and Minale model above a critical capillary number. This deviation directly corresponds to the droplet's shape transitions from ellipsoids to bullet-like shapes with tails that do not shed droplets; "rocket ships." In Fig. 9(a), a sketch of the drop shapes has been added to the data for $C=0.88$ to highlight where the drop shape transitions from ellipsoids, to bullets, to rocket ships, and finally to tail streaming. The Maffettone and Minale model fails to predict the drop deformation for the shape transitions, in part, because the model assumes ellipsoidal deformation and a constant surface tension along the drop. For fully confined droplets, the data have a very high slope leading up to a plateau where the deformation parameter seems to increase again at roughly the same slope as that predicted by the Maffettone and Minale model.

With the exception of OTAB droplets, which behave

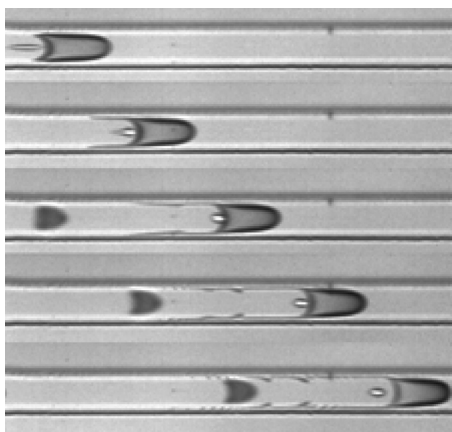


FIG. 11. Sequence of images showing the interaction of CTAB droplets within the contraction and the interesting flow structures that result.

more like water droplets, all the surfactants behave similarly to the CPyCl. As such, rather than giving extensive data sets for each surfactant a single set of confinements was chosen to compare the surfactant droplets as a function of capillary number. In Fig. 10(a), the deformation parameter is shown as a function of the capillary number for NaOa, CTAB, and CPyCl at a confinement of $C=0.77$. The NaOa and CTAB data agree well with CPyCl. Also shown is the deformation parameter as a function of capillary number for a confinement of $C=0.88$ for OTAB and CPyCl. The OTAB has much smaller deformation than the CPyCl. This is most likely due to the fact that OTAB is a very small and mobile surfactant and less likely to build up the surface tension gradients needed to induce the shape transitions and tail streaming observed for the CPyCl and other surfactants. These trends are consistent across the range of capillary numbers and confinements studied.

As an interesting aside, a series of images are presented in Fig. 11 demonstrating the dynamics and fluid structures that can occur when multiple deformed droplets can interact within a confined microfluidic channel. Here a small, strongly deformed droplet is observed in the wake of a larger droplet undergoing tail streaming. The smaller droplet is observed to move faster than the larger droplet, eventually impacting the rear of the larger droplet and bouncing off without coalescing. In addition, the tails of the large droplet are not smooth as observed for a single droplet, but contain ripples resulting from the interplay between the tails and the multiple droplets in its wake.

IV. CONCLUSIONS

The focus of this work was to understand the deformation of a single drop under pure extensional flow and mixed extensional and shear flow using a microfluidic hyperbolic contraction. Droplet formation and production is well characterized and understood. This knowledge was used to create droplets using a bottom up approach. Droplets moved through the microfluidic device to a hyperbolic contraction where they first experienced a homogeneous extensional flow and then some degree of shear flow as the droplets

became confined. Droplet deformation was only measured after droplets had reached a steady state of deformation.

Droplets were deformed by extensional forces at the entrance to the hyperbolic contraction. The deformation of both water droplets and surfactant solution droplets in an oil matrix was characterized. The droplet deformation was compared to a Maffettone and Minale model for unconfined droplets, $C < 1$, undergoing pure extensional flows. Both water and surfactant droplets followed the same trend as the Maffettone and Minale model; however, the deformation was found to grow faster than the predictions of the Maffettone and Minale model starting at a critical capillary number. This critical capillary number is found to decrease with increasing confinement and decreasing surfactant mobility. For confinements greater than $C > 1.0$, the deformation data for both the surfactant coated and clean water droplets never followed the Maffettone and Minale model. In some cases the deformation can be as much as three times that predicted for the unconfined droplets. Water droplets also did not follow the Maffettone and Minale predictions above a confinement of $C=1.0$. Droplet deformation increased with increasing confinement and was greater than that predicted by the Maffettone and Minale model which does not include confinement in its prediction of droplet deformation.

For the capillary numbers and confinements tested, the water droplets did not break up when undergoing the extensional flow as the critical capillary number for drop breakup was not reached. The shape of deformed water droplets did, however, show a smooth transition from ellipsoids to bullets, to bullet-like shapes with two elongated tails resembling a rocket ship, and then finally to tail streaming in all cases except for the OTAB. OTAB was also not observed to follow the same trends as the other surfactant solutions when droplet deformation was plotted as a function of capillary number at a given confinement. The deformation of the OTAB solution was observed to be much smaller than that for the other surfactant solutions. The evolution of the droplet shapes, for the other three surfactants used, was seen to correspond to transitions in the deformation as a function of capillary number. In the case of CPyCl, as the droplet transitioned from a blunt bullet-like shape to a bullet-like shape with two elongated tails resembling a rocket ship, the droplet deformation began to deviate from the Maffettone and Minale model quickly. The critical capillary number for tail streaming to occur decreased with increasing confinement, as the shear forces acting on the droplet increased sweeping more surfactant to the trailing edge of the droplet facilitating the observed tail streaming. The critical capillary number for tail streaming also decreases as surfactant mobility decreases and surfactant size increases.

ACKNOWLEDGMENTS

The authors would like to acknowledge the University of Massachusetts Amherst Materials Research Science and Engineering Center for funding this project. We also thank the University of Massachusetts Amherst Center for Hierarchical

Manufacturing for use of their cleanroom facilities to fabricate devices.

- ¹L. Shui, J. C. T. Eijkel, and A. van den Berg, "Multiphase flow in microfluidic systems—Control and applications of droplets and interfaces," *Adv. Colloid Interface Sci.* **133**, 35 (2007).
- ²C. Zeng, H. Bissig, and A. D. Dinsmore, "Particles on droplets: From fundamental physics to novel materials," *Solid State Commun.* **139**, 547 (2006).
- ³D. J. McClements, *Food Emulsions: Principles, Practice and Techniques* (CRC, Boca Raton, 1999).
- ⁴P. Fischer and P. Erni, "Emulsion drops in external flow fields—The role of liquid interfaces," *Curr. Opin. Colloid Interface Sci.* **12**, 196 (2007).
- ⁵G. I. Taylor, "The formation of emulsions in definable fields of flow," *Proc. R. Soc. London, Ser. A* **146**, 501 (1934).
- ⁶P. Van Puyvelde, A. Vananroye, R. Cardinaels, and P. Moldenaers, "Review on morphology development of immiscible blends in confined shear flow," *Polymer* **49**, 5363 (2008).
- ⁷W. L. Olbricht, "Pore-scale prototypes of multiphase flow in porous media," *Annu. Rev. Fluid Mech.* **28**, 187 (1996).
- ⁸B. J. Bentley and L. G. Leal, "An experimental investigation of drop deformation and breakup in steady, two-dimensional linear flows," *J. Fluid Mech.* **167**, 241 (1986).
- ⁹S. L. Anna, N. Bontoux, and H. A. Stone, "Formation of dispersions using "flow focusing" in microchannels," *Appl. Phys. Lett.* **82**, 364 (2003).
- ¹⁰G. F. Christopher and S. L. Anna, "Microfluidic methods for generating continuous droplet streams," *J. Phys. D* **40**, R319 (2007).
- ¹¹E. Miller, M. Rotea, and J. P. Rothstein, "Microfluidic device incorporating closed loop feedback control for uniform and tunable production of micro-droplets and emulsions," *Lab Chip* **10**, 1293 (2010).
- ¹²J. Husny and J. J. Cooper-White, "The effect of elasticity on drop creation in T-shaped microchannels," *J. Non-Newtonian Fluid Mech.* **137**, 121 (2006).
- ¹³H. Hillborg, N. Tomczak, A. Olah, H. Schonherr, and G. J. Vancso, "Nanoscale hydrophobic recovery: A chemical force microscopy study of UV/ozone-treated cross-linked poly(dimethylsiloxane)," *Langmuir* **20**, 785 (2004).
- ¹⁴T. Nisisako, T. Torii, and T. Higuchi, "Droplet formation in a microchannel network," *Lab Chip* **2**, 24 (2002).
- ¹⁵Q. Y. Xu and M. Nakajima, "The generation of highly monodisperse droplets through the breakup of hydrodynamically focused microthread in a microfluidic device," *Appl. Phys. Lett.* **85**, 3726 (2004).
- ¹⁶S. L. Anna and H. C. Mayer, "Microscale tipstreaming in a microfluidic flow focusing device," *Phys. Fluids* **18**, 121512 (2006).
- ¹⁷A. M. Gañán-Calvo and J. M. Gordillo, "Perfectly monodisperse microbubbling by capillary flow focusing," *Phys. Rev. Lett.* **87**, 274501 (2001).
- ¹⁸A. R. Abate, A. Poitzsch, Y. Hwang, J. Lee, J. Czerwinska, and D. A. Weitz, "Impact of inlet channel geometry on microfluidic drop formation," *Phys. Rev. E* **80**, 026310 (2009).
- ¹⁹F. C. Chang and Y. C. Su, "Controlled double emulsification utilizing 3D PDMS microchannels," *J. Micromech. Microeng.* **18**, 065018 (2008).
- ²⁰R. A. De Bruijn, "Tipstreaming of drops in simple shear flows," *Chem. Eng. Sci.* **48**, 277 (1993).
- ²¹W. G. P. Mietus, O. K. Matar, C. J. Lawrence, and B. J. Briscoe, "Droplet deformation in confined shear and extensional flow," *Chem. Eng. Sci.* **57**, 1217 (2002).
- ²²W. L. Olbricht and D. M. Kung, "The deformation and breakup of liquid-drops in low Reynolds-number flow through a capillary," *Phys. Fluids* **4**, 1347 (1992).
- ²³J. C. Baret, F. Kleinschmidt, A. El Harrak, and A. D. Griffiths, "Kinetic aspects of emulsion stabilization by surfactants: A microfluidic analysis," *Langmuir* **25**, 6088 (2009).
- ²⁴W. J. Milliken, H. A. Stone, and L. G. Leal, "The effect of surfactant on the transient motion of Newtonian drops," *Phys. Fluids A* **5**, 69 (1993).
- ²⁵K. B. Migler, "String formation in sheared polymer blends: Coalescence, breakup, and finite size effects," *Phys. Rev. Lett.* **86**, 1023 (2001).
- ²⁶A. Vananroye, P. Van Puyvelde, and P. Moldenaers, "Effect of confinement on the steady-state behavior of single droplets during shear flow," *J. Rheol.* **51**, 139 (2007).
- ²⁷J. A. Pathak and K. B. Migler, "Droplet-string deformation and stability during microconfined shear flow," *Langmuir* **19**, 8667 (2003).
- ²⁸C. Fischer, C. J. G. Plummer, V. Michaud, P.-E. Bourban, and J.-A. E. Manson, "Pre- and post-transition behavior of shear-thickening fluids in oscillating shear," *Rheol. Acta* **46**, 1099 (2007).
- ²⁹A. Vananroye, P. Van Puyvelde, and P. Moldenaers, "Effect of confinement on droplet breakup in sheared emulsions," *Langmuir* **22**, 3972 (2006).
- ³⁰C. J. Pipe and G. H. McKinley, "Microfluidic rheometry," *Mech. Res. Commun.* **36**, 110 (2009).
- ³¹G. C. Randall, K. M. Schultz, and P. S. Doyle, "Methods to electrophoretically stretch DNA: Microcontractions, gels, and hybrid gel-microcontraction devices," *Lab Chip* **6**, 516 (2006).
- ³²M. S. N. Oliveira, M. A. Alves, F. T. Pinho, and G. H. McKinley, "Viscous flow through microfabricated hyperbolic contractions," *Exp. Fluids* **43**, 437 (2007).
- ³³J. R. Anderson, D. T. Chiu, R. J. Jackman, O. Cherniavskaya, J. C. McDonald, H. K. Wu, S. H. Whitesides, and G. M. Whitesides, "Fabrication of topologically complex three-dimensional microfluidic systems in PDMS by rapid prototyping," *Anal. Chem.* **72**, 3158 (2000).
- ³⁴J. C. McDonald and G. M. Whitesides, "Poly(dimethylsiloxane) as a material for fabricating microfluidic devices," *Acc. Chem. Res.* **35**, 491 (2002).
- ³⁵L. E. Rodd, J. J. Cooper-White, D. V. Boger, and G. H. McKinley, "Role of the elasticity number in the entry flow of dilute polymer solutions in micro-fabricated contraction geometries," *J. Non-Newtonian Fluid Mech.* **143**, 170 (2007).
- ³⁶L. E. Rodd, T. P. Scott, D. V. Boger, J. J. Cooper-White, and G. H. McKinley, "The inertio-elastic planar entry flow of low-viscosity elastic fluids in micro-fabricated geometries," *J. Non-Newtonian Fluid Mech.* **129**, 1 (2005).
- ³⁷A. E. Everage and R. L. Ballman, "The extensional flow capillary as a new method for extensional viscosity measurement," *Nature (London)* **273**, 213 (1978).
- ³⁸D. F. James and G. M. Chandler, "Measurement of the extensional viscosity of M1 in a converging channel rheometer," *J. Non-Newtonian Fluid Mech.* **35**, 445 (1990).
- ³⁹D. F. James and G. M. Chandler, "A converging channel rheometer for the measurement of extensional viscosity," *J. Non-Newtonian Fluid Mech.* **35**, 421 (1990).
- ⁴⁰P. L. Maffettone and M. Minale, "Equation of change for ellipsoidal drops in viscous flow," *J. Non-Newtonian Fluid Mech.* **78**, 227 (1998).
- ⁴¹E. Miller, C. Clasen, and J. P. Rothstein, "The effect of step-stretch parameters on capillary breakup extensional rheology (CaBER) measurements," *Rheol. Acta* **48**, 625 (2009).
- ⁴²L. G. Leal, *Laminar Flow and Convective Transport Processes: Scaling Principles and Asymptotic Analysis* (Butterworth-Heinemann, Boston, 1992).
- ⁴³C. D. Eggleton, T. M. Tsai, and K. J. Stebe, "Tip streaming from a drop in the presence of surfactants," *Phys. Rev. Lett.* **87**, 048302 (2001).
- ⁴⁴M. R. Booty and M. Siegel, "Steady deformation and tip-streaming of a slender bubble with surfactant in an extensional flow," *J. Fluid Mech.* **544**, 243 (2005).
- ⁴⁵H. A. Stone, "Dynamics of drop deformation and breakup in viscous fluids," *Annu. Rev. Fluid Mech.* **26**, 65 (1994).
- ⁴⁶J. K. Ferri and K. J. Stebe, "Which surfactants reduce surface tension faster? A scaling argument for diffusion-controlled adsorption," *Adv. Colloid Interface Sci.* **85**, 61 (2000).